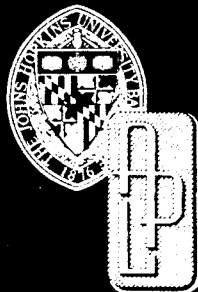AD-A247 019

JHU/APL
TG 1379
AUGUST 1991

Technical Memorandum

COMPARISON OF VARIOUS TECHNIQUES IN THE ANALYSIS OF WAVEGUIDE TRANSITIONS

W. A. HUTING

DTIC
ELECTE
S MAR 0 4 1992
B D

92-04917

THE JOHNS HOPKINS UNIVERSITY ■ APPLIED PHYSICS LABORATORY

92 2 25 153

REPORT DOCUMENTATION PAGE

1a. REPORT SECURITY CLASSIFICATION UNCLASSIFIED		1b. RESTRICTIVE MARKINGS N.A.
2a. SECURITY CLASSIFICATION AUTHORITY N.A.		3. DISTRIBUTION/AVAILABILITY OF REPORT UNCLASSIFIED/UNLIMITED
2b. DECLASSIFICATION/DOWNGRADING SCHEDULE N.A.		
4. PERFORMING ORGANIZATION REPORT NUMBER(S) JHU/APL TG-1379		5. MONITORING ORGANIZATION REPORT NUMBER(S) JHU/APL TG-1379

6a. NAME OF PERFORMING ORGANIZATION The Johns Hopkins University Applied Physics Laboratory	6b. OFFICE SYMBOL (If applicable) N.A.	7a. NAME OF MONITORING ORGANIZATION The Johns Hopkins University Applied Physics Laboratory
6c. ADDRESS (City, State, and ZIP Code) Johns Hopkins Road Laurel, Md. 20723-6099		7b. ADDRESS (City, State, and ZIP Code) Johns Hopkins Road Laurel, Md. 20723-6099

8a. NAME OF FUNDING/SPONSORING ORGANIZATION Dept. of the Navy Naval Sea Systems Command	8b. OFFICE SYMBOL (If applicable) N.A	9. PROCUREMENT INSTRUMENT IDENTIFICATION NUMBER N00039-89-C-5301

8c. ADDRESS (City, State, and ZIP Code)

Crystal City, Va. 22202

10. SOURCE OF FUNDING NUMBERS

PROGRAM ELEMENT NO.	PROJECT NO.	TASK NO.	WORK UNIT ACCESSION NO.
N. A.	N.A.	N.A.	N.A.

11. TITLE (Include Security Classification)

Comparison of Various Techniques in the Analysis of Waveguide Transitions (U)

12. PERSONAL AUTHOR(S)
William A. Huting

13a. TYPE OF REPORT Technical Monograph	13b. TIME COVERED FROM 89-8 TO 90-8	14. DATE OF REPORT (Year, Month, Day) 90-8-22	15. PAGE COUNT 39

16. SUPPLEMENTARY NOTATION

N.A.

17. COSATI CODES			18. SUBJECT TERMS (Continue on reverse if necessary and identify by block number)
FIELD	GROUP	SUB-GROUP	Microwaves, Waveguides, Runge-Kutta, Modes, Transmission, Transitions, Radar, Communications
N.A.	N.A.	N.A.	
N.A.	N.A.	N.A.	

19. ABSTRACT (Continue on reverse if necessary and identify by block number)

The solution of the continuous waveguide transition problem can be obtained by discretizing the boundary and applying mode-matching or by using a system of ordinary differential equations. Both approaches involve approximate representations of the boundary. When using the differential equation approach, it was found necessary to consider the transition as several sections in series in order to avoid numerical instabilities. When this is done, one may cascade using a generalized scattering matrix approach or a generalized ABCD matrix method. Results are shown comparing the accuracy of the boundary discretization approach and the differential equation approach for the Marie transducer and for linear transitions of various lengths in rectangular waveguide; experimental results are also given for the Marie transducer.

20. DISTRIBUTION/AVAILABILITY OF ABSTRACT [X] UNCLASSIFIED/UNLIMITED [ ] SAME AS RPT. [ ] DTIC USERS	21. ABSTRACT SECURITY CLASSIFICATION UNCLASSIFIED	
22a. NAME OF RESPONSIBLE INDIVIDUAL NAVPRO Security Officer	22b. TELEPHONE (Include Area Code) (301) 953-5442	22c. OFFICE SYMBOL SE

DD FORM 1473, 84 MAR

83 APR edition may be used until exhausted
All other editions are obsolete.

Technical Memorandum

COMPARISON OF VARIOUS TECHNIQUES IN THE ANALYSIS OF WAVEGUIDE TRANSITIONS

W. A. HUTING

ABSTRACT

The solution of the continuous waveguide transition problem can be obtained by discretizing the boundary and applying mode-matching or by using a system of ordinary differential equations. Both approaches involve approximate representations of the boundary. When using the differential equation approach, it was found necessary to consider the transition as several sections in series in order to avoid numerical instabilities. When this is done, one may cascade using a generalized scattering matrix approach or a generalized ABCD matrix method. Results are shown comparing the accuracy of the boundary discretization approach and the differential equation approach for the Marie transducer and for linear transitions of various lengths in rectangular waveguide; experimental results are also given for the Marie transducer.

CONTENTS

LIST OF FIGURES

1. INTRODUCTION

Numerical approaches to the continuous waveguide transition analysis and design problems have been studied for the past twenty or so years.[1-5] Recently, the author of this paper used a novel moment method technique to solve a system of ordinary differential equations describing such a transition;[4,5] this paper is basically an extension of the work described in References 4 and 5. The paper compares the differential equation method with an approach that approximates the transition as a series of discrete steps and subsequently applies mode-matching, applies these techniques to linear rectangular transitions, discusses the validity of the differential equations and associated boundary conditions, and reports experimental and numerical results for the Marie rectangular TE_{10} to circular TE_{01} mode transducer. Also included are new results regarding the sensitivity of the computed solution to the choice of cascading formulation when (as is a fairly common practice) a transition is analyzed as several sections in series in order to avoid numerical instabilities.[3,4,5]

2. METHODS OF SOLUTION

The system of differential equations used in this paper is based on the assumption that the transverse portion of the electromagnetic field in a transition can be written as a sum of the uniform waveguide mode functions corresponding to the local transition cross-section

$$E_t(x,y,z) = \sum_{m=1}^{\infty} V_m(z) e_m(x,y,z) \tag{1}$$

$$H_t(x,y,z) = \sum_{m=1}^{\infty} I_m(z) h_m(x,y,z) \tag{2}$$

where z denotes the direction of propagation, and the parameters $V_m(z)$ and $I_m(z)$ are known, respectively, as the equivalent voltages and the equivalent currents. A system of ordinary differential equations that specifies $V_m(z)$ and $I_m(z)$ was given by Reiter in 1959,[6] and methods of solution are discussed at some length in References 3, 4, and 5. These equations are

$$\frac{dV_m}{dz} = -j\beta_m Z_m I_m + \sum_{n=1}^{\infty} T_{mn} V_n \tag{3}$$

$$\frac{dI_m}{dz} = -j\frac{\beta_m}{Z_m} V_m - \sum_{n=1}^{\infty} T_{nm} I_n \tag{4}$$

Both TE and TM modes are included in Equations 3 and 4. The variable β_m denotes the wave number of the mth mode, the variable Z_m denotes the wave impedance of the

mth mode, and the "transfer coefficients" T_{mn} (which describe coupling between the two modes m and n) are given by[6]

$$T_{mn}(z) = \iint_{S(z)} \frac{de_m}{dz} \cdot e_n \, dx \, dy \tag{5}$$

The integration in Equation 5 is over the local waveguide cross-section $S(z)$. If the system of Equations in 3 and 4 is truncated and then solved for the portion of the transition between $z = z_i$ and $z = z_{i+1}$, one may specify numerical values for the associated generalized ABCD matrix

$$\begin{bmatrix} V(Z_{i+1}) \\ I(Z_{i+1}) \end{bmatrix} = \begin{bmatrix} A_i & B_i \\ C_i & D_i \end{bmatrix} \begin{bmatrix} V(Z_i) \\ I(Z_i) \end{bmatrix} \tag{6}$$

where the dimension of the square submatrices A_i, B_i, C_i, and D_i is equal to the number of modes (propagating and evanescent) included in the solution. Cascading the results for two adjacent portions of the transition may be accomplished by simple multiplication of the two ABCD matrices,[4,5] or by translating these two matrices into generalized scattering matrices and then linking them together.[3] One goal of this paper is to compare the efficacy of these two cascading approaches. The ABCD matrix approach is computationally less intensive and, therefore, initially more attractive than the scattering matrix approach.

One well-known alternative to solving the differential equations is to discretize the boundary and to apply mode-matching. The boundary discretization geometry used in this paper is depicted in Figure 1. The two uniform waveguides in Figure 1 have cross-sections equivalent to the transition cross-sections at z and $z + \Delta L$. As shown in Appendix A, the difference equation for the equivalent voltages and currents is

$$V_m(z + \Delta L) =$$

$$\cos\left(\frac{\beta_m \Delta L}{2}\right) \sum_{n=1}^{\infty} \cos\left(\frac{\beta_n \Delta L}{2}\right) \left(\iint_S e_n(z) \cdot e_m(z + \Delta L) dx \, dy \right) V_n(z)$$

$$- \cos\left(\frac{\beta_m \Delta L}{2}\right) \sum_{n=1}^{\infty} j Z_n(z) \sin\left(\frac{\beta_n \Delta L}{2}\right) \left(\iint_S e_n(z) \cdot e_m(z + \Delta L) dx \, dy \right) I_n(z)$$

$$+ j Z_m(z + \Delta L) \sin\left(\frac{\beta_m \Delta L}{2}\right) \sum_{n=1}^{\infty} \frac{j}{Z_n(z)} \sin\left(\frac{\beta_n \Delta L}{2}\right)$$

$$\left(\iint_S e_n(z) \cdot e_m(z + \Delta L) dx \, dy \right) V_n(z)$$

2

$$-jZ_m(z+\Delta L)\sin\left(\frac{\beta_m \Delta L}{2}\right)\sum_{n=1}^{\infty}\cos\left(\frac{\beta_n \Delta L}{2}\right)$$

$$\left(\iint_S e_n(z)\cdot e_m(z+\Delta L)dx\,dy\right)I_n(z)$$

$$(7)$$

where the area of integration S is equal to the intersection of $S(z)$ and $(z+\Delta L)$. Rewriting Equation 7 as a sum of powers of ΔL and retaining only terms of order $(\Delta L)^2$ or lower, one obtains

$$V_m(z+\Delta L) = V_m(z)$$

$$-j\Delta L\, Z_m(z)\beta_m(z)I_m(z)$$

$$+\Delta L\sum_{n=1}^{\infty}\left(\iint_S e'_m(z)\cdot e_n(z)dx\,dy\right)V_n(z)$$

$$-(\Delta L)^2\frac{(\beta_m(z))^2}{4}V_m(z)$$

$$-j(\Delta L)^2 Z'_m(z)\left(\frac{\beta_m(z)}{2}\right)I_m(z)$$

$$(8)$$

$$+\frac{(\Delta L)^2}{2}\sum_{n=1}^{\infty}\left(\iint_S e''_m(z)\cdot e_n(z)dx\,dy\right)V_n(z)$$

$$-j(\Delta L)^2\sum_{n=1}^{\infty}\left(Z_n(z)\frac{\beta_n(z)}{2}+Z_m(z)\frac{\beta_m(z)}{2}\right)$$

$$\left(\iint_S e'_m(z)\cdot e_n(z)dx\,dy\right)I_n(z)$$

where the primes refer to differentiation with respect to z. A similar equation exists for I_m. Clearly, in the limit of vanishing ΔL, Equation 8 reduces to Equation 3. Therefore, one might expect that the boundary discretization method should converge to the same solution as does the differential equation method. Convergence rates can be affected

by the $(\Delta L)^2$ terms, however, and these terms do, in fact, differ between Equation 8 and some of the techniques for solving Equations 3 and 4 (e.g., the Runge-Kutta method, discussed in Appendix B. Similar difference equations can be derived when traveling waves are considered instead of the equivalent voltages and currents of Equations 1 and 2 (further details are given in Appendix C). The mode-matching approach used in this paper[7] is a modification of the method described by Carin, Webb, and Weinreb.[8] The scattering matrix cascading technique described by Chu and Itoh[9] is used to link together the large number of junctions used to approximate a transition.

Although Equations 3 and 8 indicate that the differential equation method and the boundary discretization method should converge to a common solution, the two methods are based on somewhat different representations of the transition boundary. The differential equation approach assumes a perfectly smooth boundary, while the mode-matching approach uses a stepped boundary. It may not be correct to say that the stepped boundary is a valid approximation of the smooth boundary. This is well illustrated if one attempts to approximate the diagonal of a unit square as a series of steps: the approximate boundary will have a length equal to two, independent of the number of steps, whereas the actual diagonal has a length equal to $\sqrt{2}$. Nonetheless, in spite of these two rather different boundary representations, Equations 3 and 8 appear to indicate that the two methods are equivalent. This can perhaps be explained as follows. Most standard methods for solving Equation 3 can be written as difference equations similar to Equation 8. Any difference equation approach for solving Equation 3 will include terms of $(\Delta L)^2$ and higher, and, for nonzero ΔL, these higher order terms will represent a distortion of the smooth system of Equation 3. This distortion vanishes as ΔL vanishes, resulting in the equivalence of Equations 3 and 8. Yet another interesting issue is whether or not Equations 1 and 2 are appropiate for nonuniform waveguides. This will be discussed in Section 4.0.
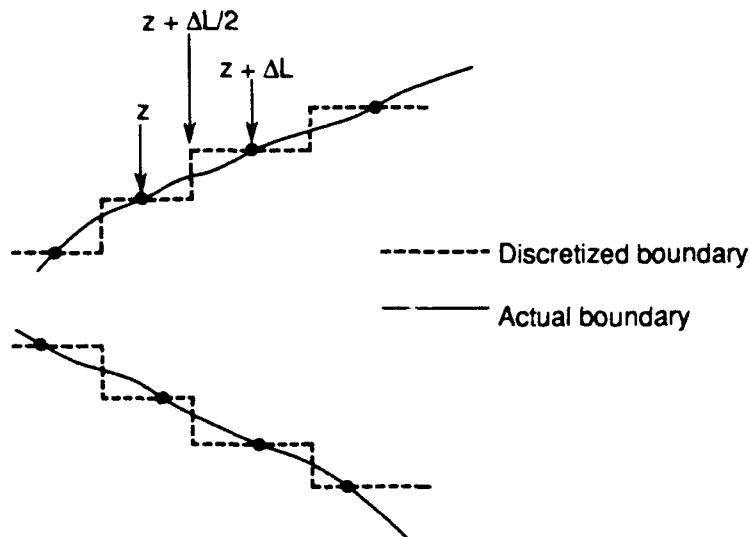
Figure 1. Boundary discretization geometry.

3.0 MARIE TRANSDUCER ANALYSIS

In this section, the numerical techniques described previously are applied to an X-band model of the Marie rectangular TE_{10} to circular TE_{01} mode transducer,[10] and the resultant data are compared with experimental results. This device, which has been informally described as "the best transition to TE_{01},"[11] is shown in Figure 2, and the desired electric field lines at various locations are shown in Figure 3. (The circular taper portion in Fig. 2 is not included in some models.)

A detailed study of the Marie transducer was performed by Saad, Davies, and Davies in the 1970s.[1,2,12] One difference between their work and ours is that they numerically implemented Solymar's small coupling procedure,[13] while we use the methods described in References 4 and 5. A prerequisite for analyzing a continuous waveguide transition is to obtain the mode functions in Equations 1 and 2. These modal solutions and the associated eigenvalues are essential in determining the coefficients in Reiter's equations.[4,6] As noted in Reference 12, these tasks must be accomplished numerically when one considers an irregularly shaped device such as the Marie transducer. The publicly available software we used is described in References 14 and 15, and further details regarding our particular implementation can be found in Reference 7. In the circular taper portion of the transition, the coefficients for the differential equations may be determined analytically.[16]

The generation of numerical data describing the transmission and reflection properties of this device will now be described. These data will be compared with measurements performed on two Marie transducers connected to each other by a 35-inch long metallic circular waveguide, i.e., launching and detecting at the two rectangular ports. Each Marie transducer was 46.35 inches long with circular taper
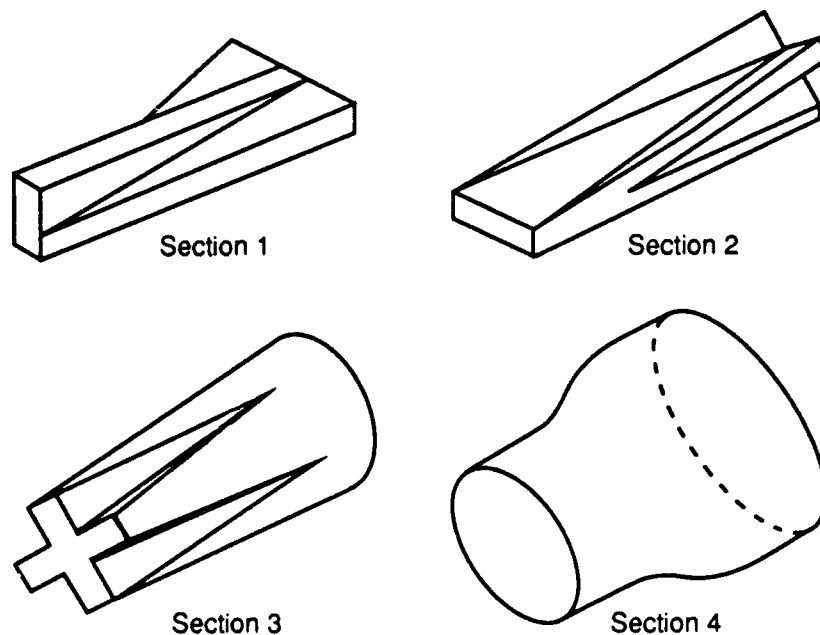
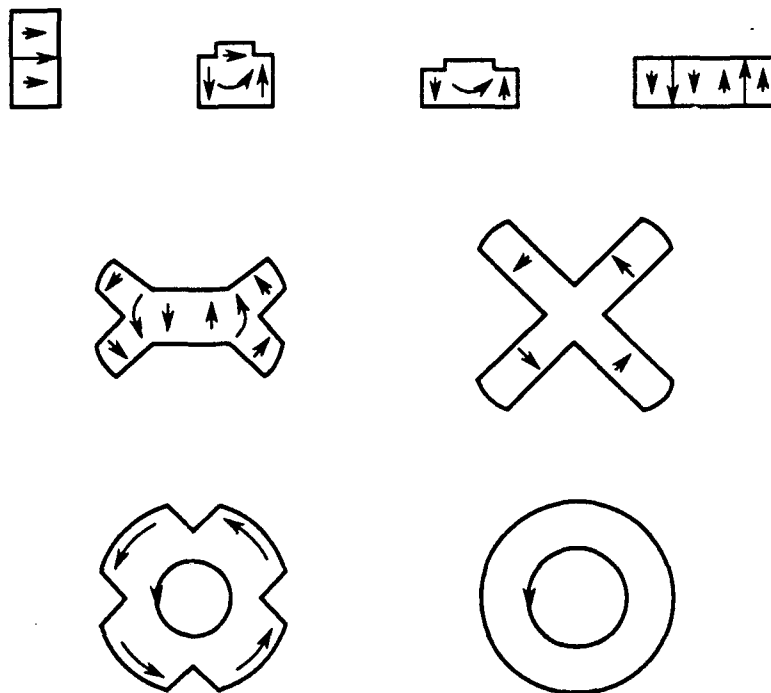

Figure 2. The Marie transducer.

**Figure 3.** Desired electric field lines for the Marie transducer.

portions, each 11 inches long. The circular ends of the Marie transducer were 1.18 inches in radius, and the rectangular ends were standard WR-90 waveguide. The numerical data were acquired using the following four schemes:

Approach 1. In the irregularly shaped portions of the Marie transducer, only the desired rectangular TE_{10}—circular TE_{01} mode is included in the expansions of Equations 1 and 2, and, in the most narrow part of the circular taper, only the desired TE_{01} mode was considered. Only a single mode was considered because previous work indicates that considering only modes near or above cutoff is sufficiently accurate while it reduces computational complexity.[4] All of these "one-mode" sections were analyzed using the Runge-Kutta technique to solve the truncated system of differential equations.[4] In a middle 1-inch portion of the taper, where the unwanted TE_{02} mode goes through cutoff, both this mode and the TE_{01} mode were included and the moment method of Reference 4 was used. The reason for selecting this technique is that, as observed in References 3 and 4, evanescent modes cause numerical problems, and the results reported in Reference 4 seem to indicate that the moment method technique has better stability characteristics than do some conventional techniques (e.g., the Runge-Kutta method and an iterative integration technique[4,5]). Finally, in the widest part of the taper, where both modes were above cutoff, the numerically less expensive Runge-Kutta technique was used. As in Reference 4, cascading was accomplished through the simple multiplication of the generalized ABCD matrices representing adjacent cross-sections. First, the 4×4 TE_{01}—TE_{02} ABCD matrices representing the circular waveguide and the wider portions of the circular tapers of the two Marie transducers were combined to produce a 4×4 ABCD matrix. The four elements of this matrix describing TE_{01} to TE_{01} interaction were used to produce a 2×2 ABCD matrix, which

was then cascaded with the "single-mode" sections. This new 2×2 matrix was then translated into a 2×2 scattering matrix. (For further details, see Chapter 4 of Ref. 7.)

In order to verify these calculations, measurements were performed using a Wiltron 360 Network Analyzer set to operate between 11 and 12 GHz. These tests included a calibration procedure that enabled normalization of the test data in the presence of imperfect connections, cables, etc., between the unit under test and the network analyzer input and output ports. (To further establish the validity of these tests, all measurements were repeated several times, and tests were performed on known devices. We believe that the $|S_{21}|$ data are accurate to within ±0.01 dB and $|S_{11}|$ to within ±10.0 dB. (For further details, see Appendix D.) Figure 4 shows numerical and experimental data for the scattering parameter S_{21} for the two Marie transducers and the connecting circular waveguide. Figure 5 shows the results for S_{11}. The experimental data indicate very low but observable dissipative loss.

Approach 2. The second method of analysis differed from Approach 1 in only one respect: cascading. The individual 4×4 ABCD matrices were converted into 4×4 scattering matrices before cascading. Chu and Itoh have published a method for cascading two devices represented by generalized scattering matrices and connected by a uniform waveguide.[9] In cascading two adjacent portions of the transition, this method was used with the length of the uniform waveguide set equal to zero in the computer program. Once the "two-mode" sections were cascaded, the four elements of the generalized scattering matrix representing TE_{01} to TE_{01} interaction were used to produce a 2×2 scattering matrix, which was then cascaded with the "single-mode" sections. Cascading such 2×2 matrices is a trivial task, and was done according to a technique described in Reference 17. Figures 6 and 7 show the data generated using this approach along with the experimental data from Figures 4 and 5.
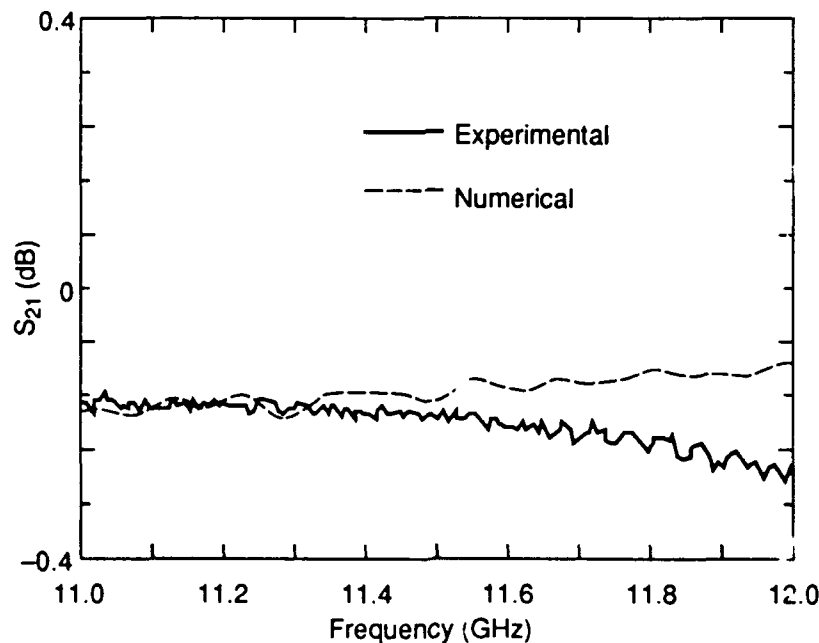
Figure 4. Experimental and numerical $|S_{21}|$ for system consisting of two Marie transducers connected by a circular waveguide. These data were generated using the ABCD matrix cascading formulation (Approach 1 in text).
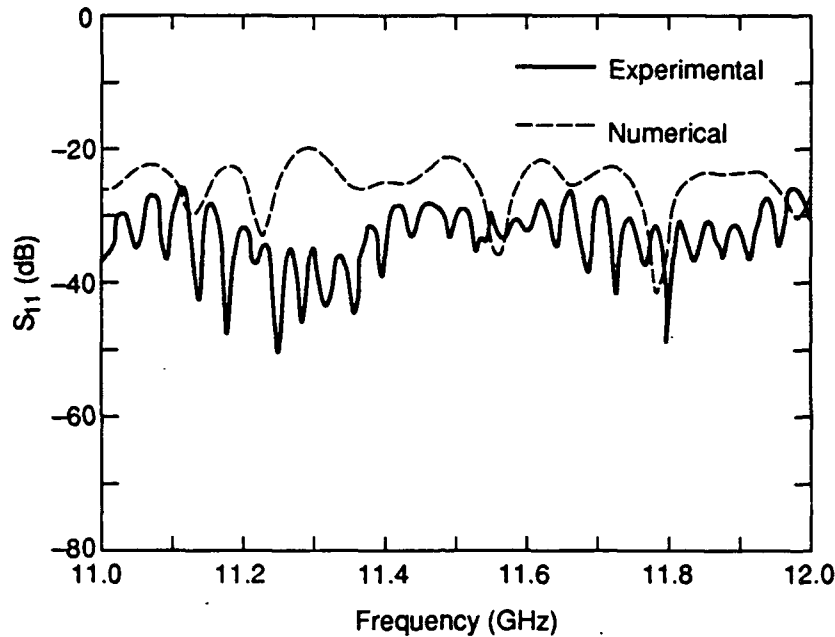
Figure 5. Experimental and numerical $|S_{11}|$ for system consisting of two Marie transducers connected by a circular waveguide. These data were generated using the ABCD matrix cascading formulation (Approach 1 in text).

Approach 3. The third approach differed from Approach 2 in only one respect: the middle part of the circular taper was analyzed using boundary discretization and mode-matching. Five modes were considered at five junctions and the resultant scattering matrix was converted into a two-mode scattering matrix (by simple truncation) before cascading with the other "two-mode" sections. Results obtained using this approach were identical to those of Approach 2, (i.e., Figures 6 and 7).

Approach 4. Boundary discretization and mode-matching were used to analyze the entire circular taper. Nine modes were used at each junction and the taper was approximated by fifty junctions. A 2 x 2 scattering matrix was extracted from the results and cascaded with the irregularly shaped "single-mode" sections. These results were very close to those of Approaches 2 and 3 (i.e., the thin lines in Figures 6 and 7).

Figures 4 through 7 show that, at least for this example, the computed solution is insensitive to whether the differential equation technique or the mode-matching technique is used. However, this is not true regarding the choice of cascading method. One might conclude that the ABCD matrix multiplication technique used in Approach 1 provided a more accurate solution than the scattering matrix cascading technique used in the other three approaches, because the numerical and experimental curves are more closely coincident in Figures 4 and 5 than in Figures 6 and 7. It should be noted, however, that these calculations do not take into account conductive losses; a "good" solution would therefore show insertion losses slightly less than those in the experiment. If observable losses are expected, the scattering matrix cascading data of Figures 6 and 7 appear more credible than the Approach 1 data of Figures 4 and 5. Further, in this case the scattering matrix formulation involved manipulating 2 x 2 submatrices with condition numbers in the range 10^0 to 10^2, while the generalized ABCD matrix formulation involved manipulating 4 x 4 matrices with condition numbers of 10^5. To

8
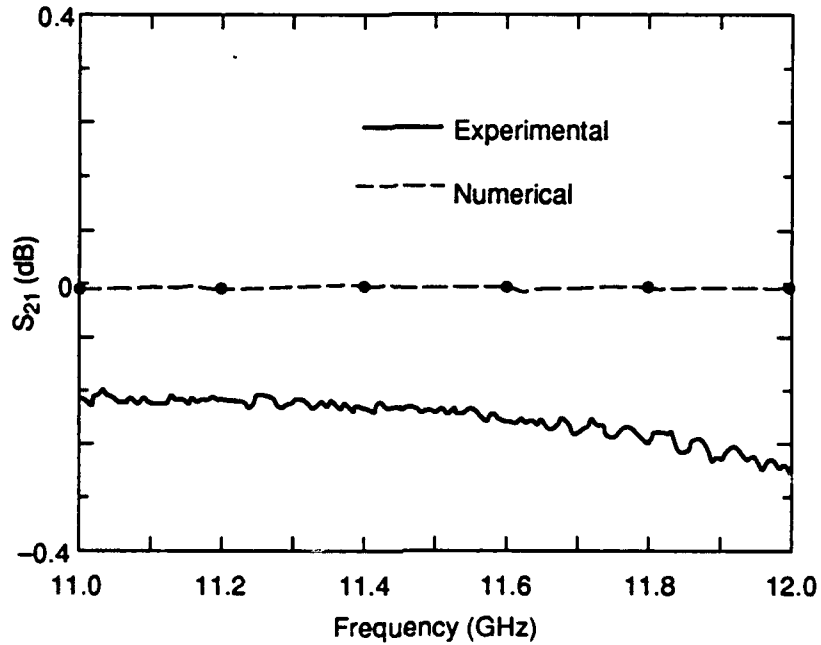
Figure 6. Experimental and numerical $|S_{21}|$ for system consisting of two Marie transducers connected by a circular waveguide. These data were generated using the scattering matrix cascading formulation (Thin line: Approaches 2 and 3 in text; dotted line: Approach 4 in text.)
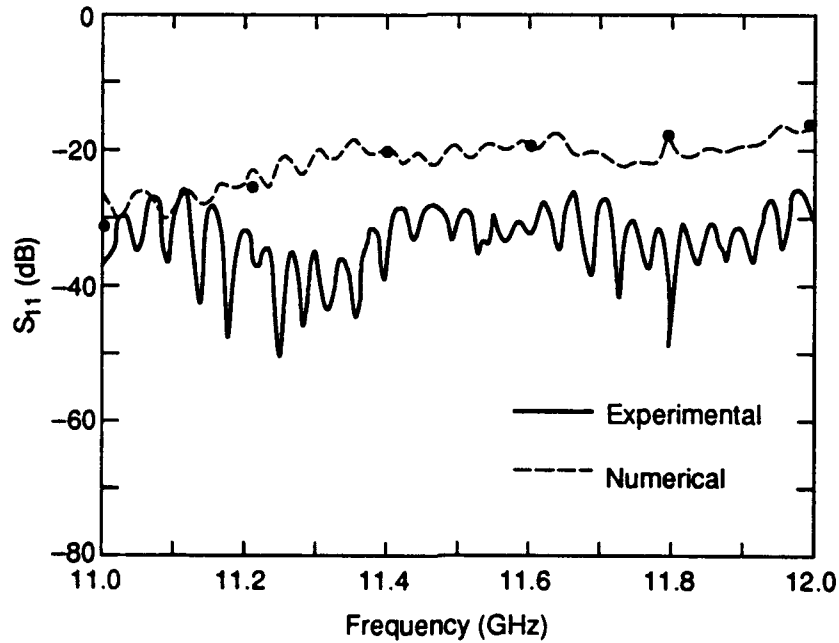
Figure 7. Experimental and numerical $|S_{11}|$ for system consisting of two Marie transducers connected by a circular waveguide. These data were generated using the scattering matrix cascading formulation (Thin line: Approaches 2 and 3 in text; dotted line: Approach 4 in text.)

sum up, for this particular example, the scattering matrix formulation utilized smaller and better conditioned matrices and yielded physically more reasonable results than does the ABCD matrix formulation.

A comparison of computer run times for the moment-method program and the mode-matching program used in the preceding examples indicates no substantial advantage from the viewpoint of computational efficiency. A similar conclusion is reached when these programs are used to analyze a simple rectangular taper.[7] It should be noted that neither of these two programs has yet been optimized with respect to either run time or storage. The Runge-Kutta technique is by far the least expensive of the methods considered here, and, as indicated in Reference 4, it is sufficiently accurate in many cases.

4. CONTINUOUS VERSUS DISCRETE FORMULATIONS

In Section 3, our particular implementations of the differential equation approach and the boundary discretization approach yielded virtually identical results when applied to the circular taper portion of a Marie transducer. This taper varies slowly with respect to wavelength. It also has been reported that the two approaches yield identical data for a slowly varying rectangular taper[7] and several extremely slowly varying circular tapers.[3] In this section, we show that the routines are also consistent for rapidly varying transitions. Our treatment starts with the rectangular taper of Figure 8 with the taper length L as a parameter. This taper is analyzed for extremely short lengths L using the previously described techniques. The $L = 0$ case, which is simply an abrupt discontinuity, is analyzed using a single-step mode-matching routine. (The differential equation technique clearly will not work for $L = 0$.) The idea is to see whether or not, for diminishing lengths L, the waveguide transition data approaches the abrupt discontinuity results and to compare the differential equation data to the boundary discretization data for these nonzero lengths L.

Figure 8 shows a transition between two rectangular waveguides with different heights. For the dimensions given, we shall consider the band between 1.0 and 1.8 GHz, where only the TE_{10} mode is capable of propagation. The abrupt ($L = 0$) case was analyzed using two methods, namely, a nine-mode mode-matching solution and a
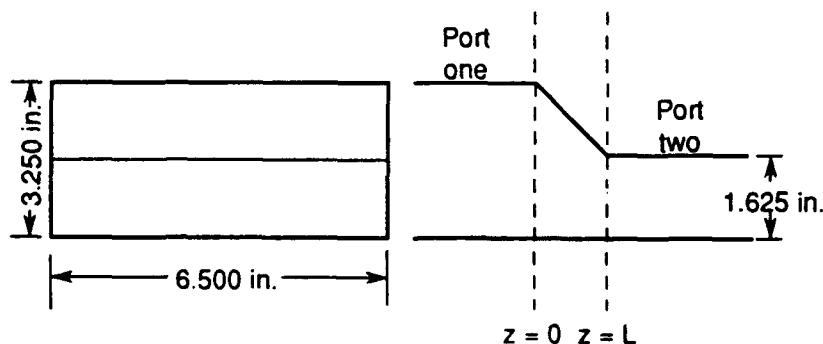

Figure 8. Steep rectangular waveguide taper.

simple procedure used data from Figure 5.26-3 in Marcuvitz's book.[18] Figure 9 shows the dominant mode reflection coefficient S_{11} obtained by these two methods and that the two sets of data are coincident. Subsequently, results were generated for the lengths $L = 0.05\lambda_0$, $0.025\lambda_0$, $0.001\lambda_0$, and $10^{-9}\lambda_0$, where λ_0 is the free-space wavelength at 1.0 GHz. These results were generated taking into account the nine lowest modes and by using two analytical techniques. First, boundary discretization and mode-matching were applied with 100 junctions between $z = 0$ and $z = L$. Second, the Galerkin's method version of the moment-method technique[4] was used with two cascaded sections between $z = 0$ and $z = L$, and with five triangle weighting functions per section. For each length, both sets of curves were indistinguishable; these curves are shown in Figure 10. The results for $L = 10^{-9}\lambda_0$ are very close to the $L = 0$ results shown in Figure 9 generated by using a nine-mode, single-step, mode-matching routine.

For the short transition example just described, the differential equation technique and the boundary discretization technique are in agreement, just as they were for
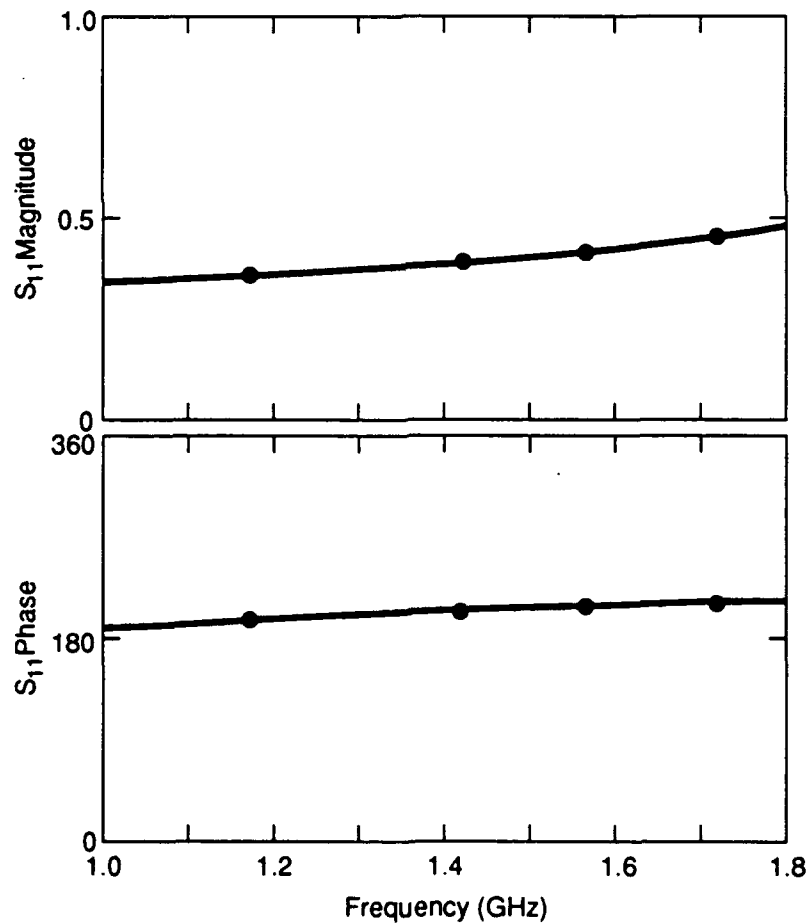
Figure 9. Computed reflection coefficient for the steep taper of Figure 7 for the abrupt discontinuity (L = 0) case. The solid line was generated using mode-matching with nine modes. The dots were generated using Fig. 5.26-3 from Reference 18.

gradual tapers. Indeed, consistency between these two methods is what one would expect after examining Equations 3 and 8. This agreement between the two techniques might be theoretically important. This is because, as observed in Reference 19, the magnetic field expansion (Equation 2) cannot satisfy the transition wall boundary condition exactly. At the wall, the magnetic field must satisfy (see Fig. 11):

$$\mathbf{H} \cdot \mathbf{m} = 0 \tag{9}$$

The individual terms of the expansion satisfy:

$$\mathbf{h}_m \cdot \mathbf{n} = 0 \tag{10}$$

(The boundary condition for the electric field is satisfied by the individual terms of Equation 1.) If the transition is a slowly varying (i.e., nearly uniform) one, Equations
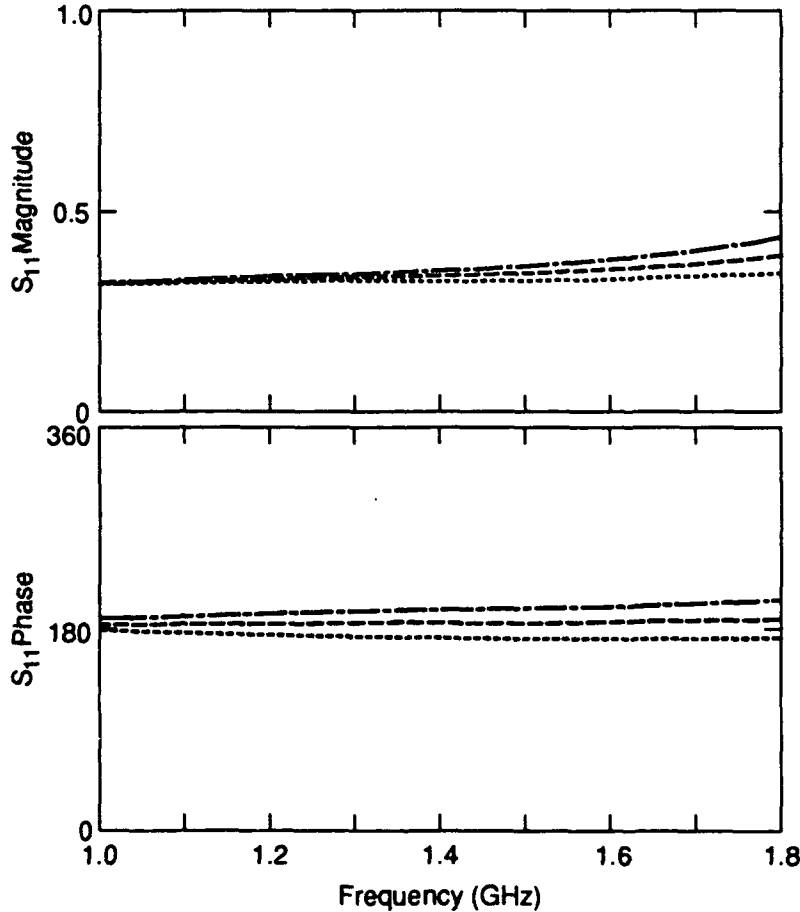
Figure 10. Computed reflection coefficient for the steep taper of Figure 7 for the cases $L = 0.05\lambda_0$ (dots), $L = 0.025\lambda_0$ (dash), $L = 0.001\lambda_0$ (chaindot), and $L = 10^{-9}\lambda_0$ (chaindot), where is the free-space wavelength at 1.0 GHz. Each of these four sets of data was generated using the differential equation method and the boundary discretization method (nine modes). The two methods yielded identical results.

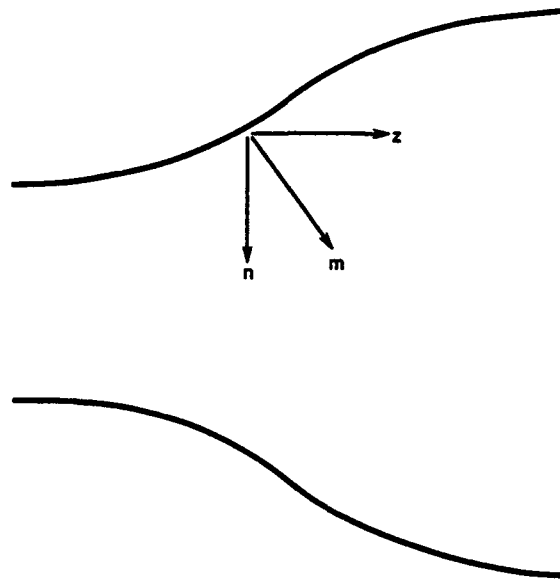**Figure 11. Waveguide transition geometry for electromagnetic boundary conditions.**

9 and 10 are approximately the same, but for rapidly varying tapers, the unit vectors m and n become less coincident, the approximation breaks down, and one might question the validity of the differential equation method. For the steep taper in Figure 8, however, the differential equation method yields the same results as the boundary discretization technique, and these two idential sets of results converge to the abrupt discontinuity solution for diminishing values of L. Moreover, consistency among these same techniques when applied to a steep circular waveguide taper has also been reported (see Appendix E). Thus, the differential equation formulation appears to be suitable even for rapidly varying tapers. One possible explanation for this may be found in an idea advanced by Unger,[19] namely, that the expansion Equation 2 is valid, that it converges to the correct field values inside but not on the boundary, and that this expansion therefore suffers a discontinuity on the boundary. Recently, it has been argued that the mathematics of the derivation of Reiter's equations are fully consistent with the existence of an expansion with these attributes (Ref. 7).

5. CONCLUSION

Several waveguide transitions have been analyzed using two different methods, discretizing the transition boundary and using mode-matching, and by solving a system of ordinary differential equations. For gradual transitions, the two methods lead to identical results and use comparable amounts of computer time (assuming the same number of modes is used in both cases). For extremely steep transitions (excluding the step transition), our results still indicate agreement between the two methods. Our results also indicate that the scattering matrix cascading method (previously used by Flugel and Kuhn[3]) leads to results that are more credible than those obtained when cascading is performed by multiplying generalized ABCD matrices. The differential equation technique may be more generally applicable for continuous transitions in that artificial discontinuities are not introduced, and an arbitrary number (including zero) of evanescent modes can be introduced.

ACKNOWLEDGMENTS

REFERENCES

[1]Saad, S. S., Davies, J. B., and Davies, O. J., "Analysis and Design of a Circular TE_{01} Mode Transducer," *IEEE Journal on Microwaves, Optics, and Acoustics,* Volume 1, 58-62 (Jan 1977).

[2]Saad, S. S., Davies, J. B., and Davies, O. J., "Computer Analysis of Gradually Tapered Waveguide with Arbitrary Cross-Sections," *IEEE Transactions on Microwave Theory and Techniques,* Volume MTT-25, 437-440 (May 1977).

[3]Flugel, H., and Kuhn, E., "Computer-Aided Analysis and Design of Circular Waveguide Tapers," *IEEE Transactions on Microwave Theory and Techniques,* Volume MTT-36, 332-336 (Feb 1988).

[4]Huting, W. A., and Webb, K. J., "Numerical Solution of the Continuous Waveguide Transition Problem," *IEEE Transactions on Microwave Theory and Techniques,* Volume MTT-37, 1802-1818 (Nov 1989).

[5]Huting, W. A., and Webb, K. J., "Numerical Analysis of Rectangular and Circular Waveguide Tapers," *IEEE Transactions on Magnetics,* Volume MAG-25, 3095-3097 (Jul 1989).

[6]Reiter, G., "Generalized Telegraphist's Equation for Waveguides of Varying Cross-Section," *Proceedings of the IEEE,* Volume 106B, Supplement 13, 54-57 (Sep 1959).

[7]Huting, W. A., "Numerical Analysis of Tapered Waveguide Transitions," Ph.D. dissertation, University of Maryland, College Park, Md. (Aug 1989).

[8]Carin, L., Webb, K. J., and Weinreb, S., "Matched Windows in Circular Waveguide," *IEEE Transactions on Microwave Theory and Techniques*, Volume MTT-36, 1359-1362 (Sep 1988).

[9]Chu, T. S., and Itoh, T. "Generalized Scattering Matrix Method for Analysis of Cascaded and Offset Microstrip Step Discontinuities," *IEEE Transactions on Microwave Theory and Techniques*, Volume MTT-34, 280-284 (Feb 1986).

[10]Marie, G. R. P., "Mode Transforming Waveguide Transition," U. S. Patent No. 2,859,412 (4 Nov 1958).

[11]Anderson, T. N., "Low Loss Transmission Using Overmoded Waveguide: A Practical 1981 Review of the State of the Art," IEEE AP/MTT-S Philadelphia Section Benjamin Franklin 1981 Symposium on Advances in Antenna and Microwave Technology, Philadelphia, Pa. (16 May 1981).

[12]Saad, S. S., "Computer Analysis and Design of Gradually Tapered Waveguide with Arbitrary Cross-Sections," Ph.D. dissertation, University College, London (Oct 1973).

[13]Solymar, L., "Spurious Mode Generation in Nonuniform Waveguide," *IEEE Transactions on Microwave Theory and Techniques*, Volume MTT-7, 379-383 (Jul 1959).

[14]Menzel, M. T., and Stokes, H. K., "User's Guide for the POISSON/SUPERFISH Group of Codes," Los Alamos National Laboratory LA-UR-87-115, Los Alamos, N. M. (Jan 1987).

[15]Konrad, A., and Silvester, P. P., "Scalar Finite-Element Package for Two-Dimensional Field Problems," *IEEE Transactions on Microwave Theory and Techniques*, Volume MTT- 19, 952-954 (Dec 1971).

[16]Sporleder, F., and Unger, H.-G., *Waveguide Tapers, Transitions, and Couplers*, New York: Peter Peregrinus (1979).

[17]Dicke, R. H., "General Microwave Circuit Theorems," in *Principles of Microwave Circuits*, Montgomery, C. G., Dicke, R. H., and Purcell, E. M. (eds.), McGraw-Hill, N.Y., 130-161 (1948).

[18]Marcuvitz, N., *Waveguide Handbook*, McGraw-Hill, New York (1951). Reprinted by Peter Pereginus, Ltd. (1986).

[19]Unger, H.-G., "Circular Waveguide Taper of Improved Design," *Bell System Technical Journal*, Volume 37, 899-912 (Jul 1958).

[20]Stevenson, A. F., "General Theory of Electromagnetic Horns," *Journal of Applied Physics*, Volume 22, 1447-1460 (Dec 1951).

[21]Ragan, G. L, *Microwave Transmission Circuits*, Dover, New York (1965).

[22]Carin, L., "Computational Analysis of Cascaded Coaxial and Circular Waveguide Discontinuities," Master's Thesis, University of Maryland, College Park, Maryland (1986).

APPENDIX A.
DERIVATION OF EQUATION 7

In Fig. A-1, the electromagnetic fields in the z-plane are given by:

$$E(z) = \sum_{n=1}^{\infty} V_n(z) e_n(z) \tag{A-1}$$

$$H(z) = \sum_{n=1}^{\infty} I_n(z) h_n(z) \tag{A-2}$$

Similarly, the fields in the $(z + \Delta L)$ plane are given by:

$$E(z + \Delta L) = \sum_{m=1}^{\infty} V_m(z + \Delta L) e_m(z + \Delta L) \tag{A-3}$$

$$H(z + \Delta L) = \sum_{m=1}^{\infty} I_m(z + \Delta L) h_m(z + \Delta L) \tag{A-4}$$

By applying the ABCD matrix for a uniform waveguide, the equivalent voltages and currents at $z + \Delta L/2$ are seen to be related to Equations A-1 and A-2 by:

$$V_n\left(z + \frac{\Delta L}{2}\right) = \cos\left(\frac{\beta_n \Delta L}{2}\right) V_n(z) - j Z_n(z) \sin\left(\frac{\beta_n \Delta L}{2}\right) I_n(z) \tag{A-5}$$
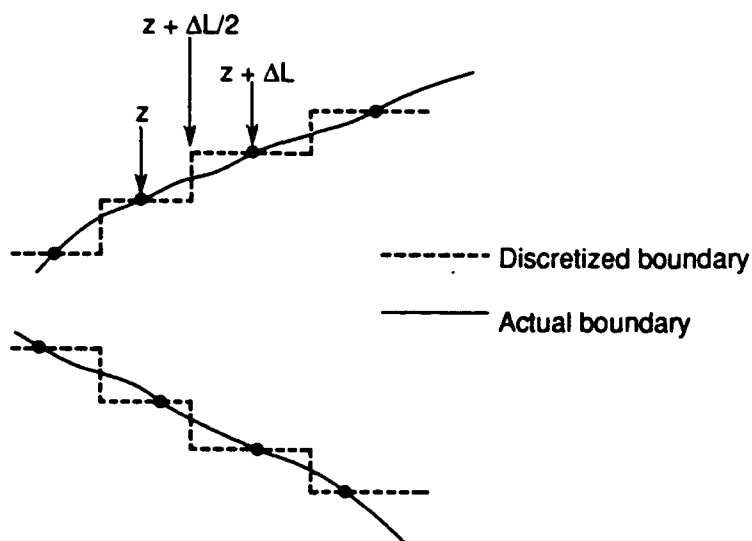
Figure A-1. Boundary discretization geometry.

$$I_n\left(z+\frac{\Delta L}{2}\right)=\frac{-j}{Z_n(z)}\sin\left(\frac{\beta_n\Delta L}{2}\right)V_n(z)+\cos\left(\frac{\beta_n\Delta L}{2}\right)I_n(z) \qquad \text{(A-6)}$$

The equivalent voltages and currents on the left sides of Equations A-5 and A-6 are the coefficients of the mode functions $e_n(z)$ and $h_n(z)$. When expanding the fields at $z+\Delta L/2$ in terms of the mode functions $e_m(z+\Delta L)$ and $h_m(z+\Delta L)$, we shall denote the corresponding coefficients $V_m(z+\Delta L/2)$ and $I_m(z+\Delta L/2)$. These new variables are related to those of Equations A-3 and A-4 by:

$$V_m(z+\Delta L)=\cos\left(\frac{\beta_m\Delta L}{2}\right)V_m\left(z+\frac{\Delta L}{2}\right)-jZ_m(z+\Delta L)\sin\left(\frac{\beta_m\Delta L}{2}\right)I_m\left(z+\frac{\Delta L}{2}\right)$$

$$\text{(A-7)}$$

$$I_m(z+\Delta L)=\frac{-j}{Z(z+\Delta L)}\sin\left(\frac{\beta_m\Delta L}{2}\right)V_m\left(z+\frac{\Delta L}{2}\right)+\cos\left(\frac{\beta_m\Delta L}{2}\right)I_m\left(z+\frac{\Delta L}{2}\right)$$

$$\text{(A-8)}$$

Enforcing the field continuity condition at $z+\Delta L/2$, one obtains:

$$\sum_{n=1}^{\infty}V_n\left(z+\frac{\Delta L}{2}\right)e_n(z)=\sum_{m=1}^{\infty}V_m\left(z+\frac{\Delta L}{2}\right)e_m(z+\Delta L) \qquad \text{(A-9)}$$

$$\sum_{n=1}^{\infty}I_n\left(z+\frac{\Delta L}{2}\right)h_n(z)=\sum_{m=1}^{\infty}I_m\left(z+\frac{\Delta L}{2}\right)h_m(z+\Delta L) \qquad \text{(A-10)}$$

Furthermore, utilizing the well known orthonormality relationships among the mode functions,

$$V_m\left(z+\frac{\Delta L}{2}\right)=\sum_{n=1}^{\infty}V_n\left(z+\frac{\Delta L}{2}\right)\iint_S e_n(z)\cdot e_m(z+\Delta L)\,dx\,dy \qquad \text{(A-11)}$$

$$I_m\left(z+\frac{\Delta L}{2}\right)=\sum_{n=1}^{\infty}I_n\left(z+\frac{\Delta L}{2}\right)\iint_S h_n(z)\cdot h_m(z+\Delta L)\,dx\,dy \qquad \text{(A-12)}$$

The remainder of the derivation is straightforward but tedious. First, one substitutes Equations A-5 and A-6 into Equations A-11 and A-12, thereby obtaining new expressions for $V_m(z+\Delta L/2)$ and $I_m(z+\Delta L/2)$. These new expressions are substituted into Equation A-7, immediately yielding Equation 7 from the main text.

$$V_m(z + \Delta L) =$$

$$\cos\left(\frac{\beta_m \Delta L}{2}\right) \sum_{n=1}^{\infty} \cos\left(\frac{\beta_n \Delta L}{2}\right) \left(\iint_S e_n(z) \cdot e_m(z + \Delta L) \, dx \, dy \right) V_n(z)$$

$$-\cos\left(\frac{\beta_m \Delta L}{2}\right) \sum_{n=1}^{\infty} j \, Z_n(z) \sin\left(\frac{\beta_n \Delta L}{2}\right) \left(\iint_S e_n(z) \cdot e_m(z + \Delta L) \, dx \, dy \right) I_n(z)$$

$$+ j Z_m(z + \Delta L) \sin\left(\frac{\beta_m \Delta L}{2}\right) \sum_{n=1}^{\infty} \frac{j}{Z_n(z)} \sin\left(\frac{\beta_n \Delta L}{2}\right)$$

$$\tag{7}$$

$$\left(\iint_S e_n(z) \cdot e_m(z + \Delta L) \, dx \, dy \right) V_n(z)$$

$$- j Z_m(z + \Delta L) \sin\left(\frac{\beta_m \Delta L}{2}\right) \sum_{n=1}^{\infty} \cos\left(\frac{\beta_n \Delta L}{2}\right)$$

$$\left(\iint_S e_n(z) \cdot e_m(z + \Delta L) \, dx \, dy \right) I_n(z)$$

Applied Physics Laboratory
Laurel, Maryland 20723-6099

APPENDIX B.
APPLICATION OF THE RUNGE-KUTTA METHOD TO EQUATION 3

$$\frac{dV_m}{dz} = -j\beta_m Z_m I_m + \sum_{n=1}^{\infty} T_{mn} V_n \qquad (3)$$

$$\frac{dI_m}{dz} = -j\frac{\beta_m}{Z_m} V_m - \sum_{n=1}^{\infty} T_{nm} I_n \qquad (4)$$

Equations 3 and 4 from the main text may be written symbolically as

$$\frac{dy}{dz} = C(z)y \qquad (B\text{-}1)$$

where:

$$y = \begin{bmatrix} V_1(z) \\ V_2(z) \\ \vdots \\ I_1(z) \\ I_2(z) \\ \vdots \end{bmatrix} \qquad (B\text{-}2)$$

and

$$C = \begin{pmatrix} T_{mn} & -j\beta_m Z_m \delta_{mn} \\ -j\frac{\beta_m}{z_m}\delta_{mn} & -T_{nm} \end{pmatrix} \qquad (B\text{-}3)$$

The Runge-Kutta method may be summarized as follows. We define the four vectors:

$$K_1 = \Delta L\, C(z)y(z) \qquad (B\text{-}4)$$

$$K_2 = \Delta L\, C\!\left(z + \frac{\Delta L}{2}\right)\!\left(y(z) + \frac{K_1}{2}\right) \qquad (B\text{-}5)$$

$$K_3 = \Delta L C \left(z + \frac{\Delta L}{2} \right) \left(y(z) + \frac{K_2}{2} \right) \qquad \text{(B-6)}$$

$$K_4 = \Delta L C \left(z + \frac{\Delta L}{2} \right) (y(z) + K_3) \qquad \text{(B-7)}$$

The estimate for $y(z + \Delta L)$ is:

$$y(z + \Delta L) = y(z) + \frac{1}{6}(K_1 + zK_2 + zK_3 + K_4) \qquad \text{(B-8)}$$

Expanding the matrix C in the form of a Taylor's series, and retaining only the terms of order $(\Delta L)^2$ or lower, one obtains for the vectors $K_1, K_2, K_3,$ and K_4:

$$K_1 = \Delta L\, C(z) y(z) \qquad \text{(B-9)}$$

$$K_2 = \Delta L\, C(z) y(z) + \frac{1}{2}(\Delta L)^2 (C(z))^2 y(z) + \frac{1}{2}(\Delta L)^2 C'(z) y(z) \qquad \text{(B-10)}$$

$$K_3 = K_2 \qquad \text{(B-11)}$$

$$K_4 = \Delta L\, C(z) y(z) + (\Delta L)^2 (C(z))^2 y(z) + (\Delta L)^2\, C'(z) y(z) \qquad \text{(B-12)}$$

Substituting these terms into Equation B-8, one obtains:

$$y(z + \Delta L) = y(z) + \Delta L\, C(z) y(z)$$

$$+ \frac{1}{2}(\Delta L)^2 (C(z))^2 y(z) \qquad \text{(B-13)}$$

$$+ \frac{1}{2}(\Delta L)^2\, C'(z) y(z)$$

The next step is to substitute the explicit expressions for y and C (Equations B-2 and B-3) into Equation B-13. This yields:

$$V_m(z + \Delta L) = V_m(z) - j\Delta L Z_m \beta_m I_m(z) + \Delta L \sum_{n=1}^{\infty} T_{mn} V_n(z)$$

$$+ \frac{1}{2}(\Delta L)^2 \left[\sum_{n=1}^{\infty} (-j\beta_n Z_n T_{mn} + j\beta_m T_{nm}) I_n(z) \right.$$

$$+ \sum_{n=1}^{\infty} \left(\sum_{k=1}^{\infty} T_{mk} T_{kn} - \beta_m^2 \delta_{mn} \right) V_n(z)$$

$$\left. -(j\beta_m' Z_m + j\beta_m Z_m') I_m(z) + \sum_{n=1}^{\infty} T_{mn}' V_n(z) \right]$$

(B-14)

The term T'_{mn} (where the prime denotes differentiation with respect to z) can be evaluated by invoking the differentiation theorem of surface integrals with variable surface (Ref. 20, main text):

$$\frac{d}{dz} \iint_{S(z)} \chi \, dx \, dy = \iint_{S(z)} \frac{\partial \chi}{\partial z} dx \, dy + \oint_{C(z)} \chi(\tan \phi) d\ell \qquad \text{(B-15)}$$

where ϕ is shown in Figure 11 and $C(z)$ is the contour defining $S(z)$. The relation can be used to show:

$$T'_{mn} = \iint_{S(z)} \frac{d^2 e_m}{dz^2} \cdot e_n dx \, dy + \iint_{S(z)} \frac{de_m}{dz} \cdot \frac{de_n}{dz} dx \, dy + \oint_{C(z)} \frac{de_m}{dz} \cdot e_n (\tan \phi) d\ell \quad \text{(B-16)}$$

Equation B-14, with the term T'_{mn} given by Equation B-16, gives the ΔL and $(\Delta L)^2$ terms for the difference equation representation of the Runge-Kutta method. The differences between this method and the boundary discretization technique are embodied in terms of order $(\Delta L)^2$ or higher — the ΔL terms are exactly the same. In the limit of vanishing ΔL, the differences between the two methods vanish and both Equations 7 (from the main text) and B-14 reduce to Equation 3 of the main text.

APPENDIX C.
TRAVELING WAVE FORMULATION OF THE
WAVEGUIDE TRANSITION PROBLEM

The forward-traveling wave coefficient $A_p^+(z)$ and the backward-traveling wave coefficient $A_p^-(z)$ are related to the equivalent voltage and equivalent current of the pth mode via the relations

$$V_p = \sqrt{Z_p}(A_p^+ + A_p^-) \tag{C-1}$$

and

$$I_p = \sqrt{Y_p}(A_p^+ - A_p^-) \tag{C-2}$$

where the modal wave admittance Y_p is the inverse of the modal wave impedance Z_p. Using the boundary discretization approach, the equations relating the wave coefficients at z and $z + \Delta L$ (Fig. 1) are:

$$\sum_{\ell=1}^{\infty} K_{p\ell}\sqrt{Z_\ell(z)}\, e^{-j\beta_\ell(z)\Delta L/2} A_\ell^+(z) - \sqrt{Z_p(z+\Delta L)}\, e^{-j\beta_p(z+\Delta L)\Delta L/2} A_p^-(z+\Delta L) =$$

$$-\sum_{\ell=1}^{\infty} K_{p\ell}\sqrt{Z_\ell(z)}\, e^{+j\beta_\ell(z)\Delta L/2} A_\ell^-(z) + \sqrt{Z_p(z+\Delta L)}\, e^{+j\beta_p(z+\Delta L)\Delta L/2} A_p^+(z+\Delta L) \tag{C-3}$$

$$\sqrt{Y_p(z)}\, e^{-j\beta_p(z)\Delta L/2} A_p^+(z) + \sum_{\ell=1}^{\infty} \sqrt{Y_\ell(z+\Delta L)}\, K_{\ell p}\, e^{-j\beta_\ell(z+\Delta L)\Delta L/2} A_\ell^-(z+\Delta L) =$$

$$\sqrt{Y_p(z)}\, e^{+j\beta_p(z)\Delta L/2} A_p^-(z) + \sum_{\ell=1}^{\infty} \sqrt{Y_\ell(z+\Delta L)}\, K_{\ell p}\, e^{+j\beta_\ell(z+\Delta L)\Delta L/2} A_\ell^+(z+\Delta L) \tag{C-4}$$

where:

$$K_{p\ell} = \iint_S \mathbf{e}_\ell(z) \cdot \mathbf{e}_p \; dx\, dy \tag{C-5}$$

In implementing Equations C-3 and C-4, a solution is obtained and scattering matrices are determined according to Reference 7 (Chap. 5). One might attempt to use the equivalent voltages and currents in conjunction with the boundary discretization approach (Equation 7), but the problem with this scheme is that the complex trigonometric functions associated with the evanescent modes will quite often exceed the numerical range of the computer. In this study this problem was circumvented by using traveling waves according to the procedure described by Chu and Itoh.[9]

The differential equations for the wave amplitudes are found by substituting Equations C-1 and C-2 into Equations 3 and 4. These equations (from Ref. 2 and 13) are:

$$\frac{dA_p^+}{dz} = -j\beta_p A_p^+ - \frac{1}{2}\frac{d(\ln Z_p)}{dz}A_p^- + \sum_{\ell=1}^{\infty}(S_{p\ell}^+ A_\ell^+ + S_{\ell p}^- A_\ell^-) \tag{C-6}$$

$$\frac{dA_p^-}{dz} = +j\beta_p A_p^- - \frac{1}{2}\frac{d(\ln Z_p)}{dz}A_p^+ + \sum_{\ell=1}^{\infty}(S_{p\ell}^- A_\ell^+ + S_{\ell p}^+ A_\ell^-) \tag{C-7}$$

where:

$$S_{p\ell}^{\pm} \equiv \frac{1}{2}\left[\sqrt{\frac{Z_\ell}{Z_p}}T_{\ell p} \mp \sqrt{\frac{Z_p}{Z_\ell}}T_{p\ell}\right] \tag{C-8}$$

In many instances, Equations C-6 and C-7 are hard to implement numerically because, if a particular mode goes through cutoff in the transition, the associated parameter $\sqrt{Z_p}$ will diverge if the mode is TE, and the associated parameter $\sqrt{Y_p}$ will diverge if the mode is TM. Therefore, in our work, we have used Equations 3 and 4 instead of Equations C-6 and C-7.

APPENDIX D.
CALCULATION OF MEASUREMENT ERRORS

As an aid in establishing rough estimates for the measurement errors in our tests, scattering parameter data were obtained for a PRD X101V rotary attenuator. This attenuator consists of a rectangular waveguide with a movable resistive card in it. If this card is oriented perpendicular to the modal electric field lines, little or no attenuation should occur. Rotation of this card away from this position increases the transmission loss, which is read from a dial. Figure D-1 shows the measured S_{21} for the settings 0.0 dB and 0.2 dB. The difference between the two sets of measured data is 0.2 dB, ± 0.01 dB. Therefore, based on these data, we make the claim that our $|S_{21}|$ data are accurate to within ± 0.01 dB.

In order to get an estimate of the error in $|S_{11}|$, we performed measurements on two rotary attenuators in series. First, measurements on all four scattering parameters were made for both phase and magnitude. In the second test, a short was placed on port 2, and the reflection coefficient was measured. We denote the reflection coefficient in the second test S_{11}. This parameter is easily shown to be related to the scattering parameters of the first test by:

$$S'_{11} = S_{11} - \frac{S_{12}S_{21}}{1 + S_{22}} \tag{D-1}$$

The relationship between the actual reflection coefficients and the measured data can be written as:

$$S'_{11} = e\, S'_{11\,meas} \tag{D-2}$$

$$S_{11} = e\, S_{11\,meas} \tag{D-3}$$

$$S_{22} = e\, S_{22\,meas} \tag{D-4}$$

Since all three measured parameters were in the same range (30 to 35 dB), it seems reasonable to postulate that e takes on the same value in all three relationships. Substituting Equations D-1, D-2, D-3, and D-4 into Equation D-1, one obtains the following equation for e:

$$S_{22\,meas}(S'_{11\,meas} - S_{11\,meas})e^2 + (S'_{11\,meas} - S_{11\,meas})e + S_{12\,meas}\,S_{21\,meas} = 0 \tag{D-5}$$

Equation D-5 has two roots, one of which oscillates in the range 30 to 40 dB between 11 and 12 GHz. Since this root would result in a reflection coefficients near 0 dB in Figures 5 and 7 (of the main text), it can be rejected as unphysical. The other root is shown as a function of frequency in Figure D-2. From these data, the calculated error in $|S_{11}|$, is seen to be within ± 10.0 dB. Perhaps not coincidently, this is the magnitude of the oscillations in the data of Figures 5 and 7.

Finally, it should be noted that these error bounds are somewhat greater than those described in the Wiltron 360 manual. One possible reason for this is that the efficacy

of the calibration procedure can be degraded due to faulty cables and connectors even if the network analyzer is in excellent condition.

S_{21} Forward Transmission
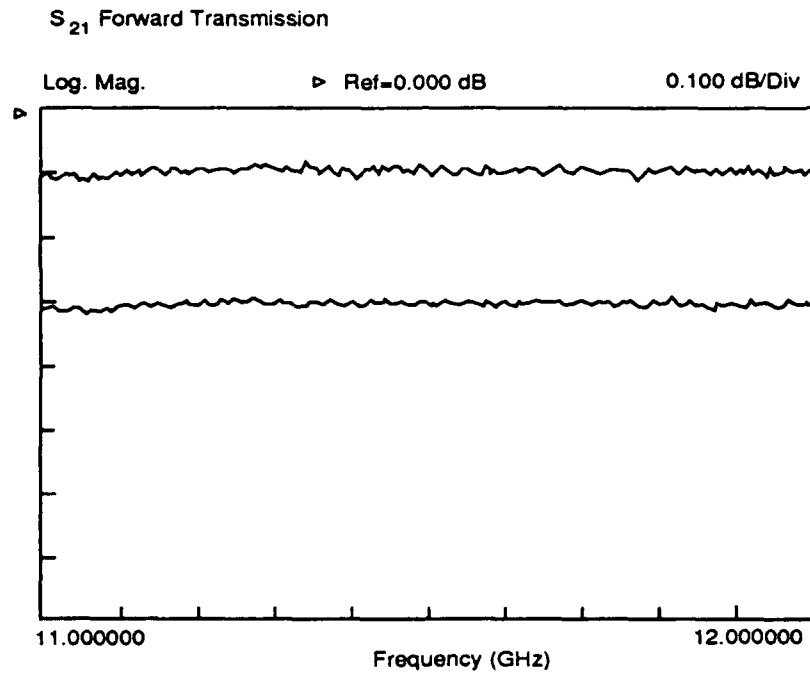
Figure D-1. Measured $|S_{21}|$ for a precision rotary attenuator. Top line: Attenuator setting at 0.0 dB. Bottom line: Attenuator setting at 0.2 dB.
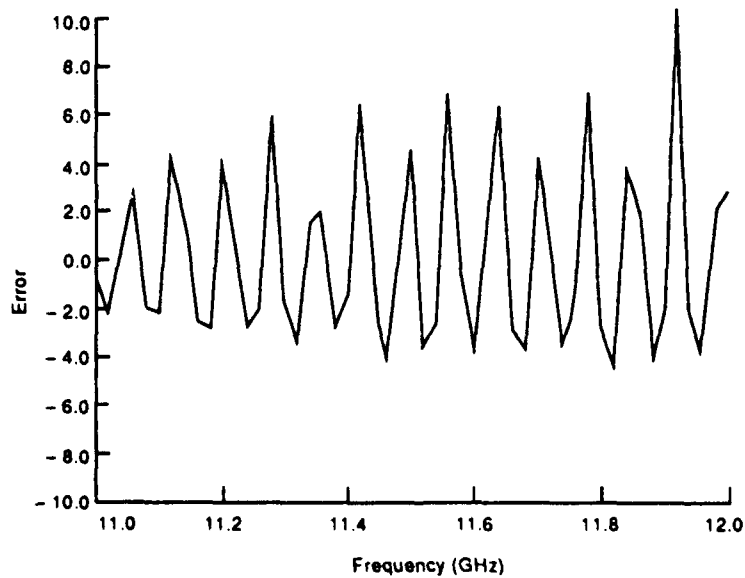
Figure D-2. Estimated error in $|S_{11}|$.

APPENDIX E.
NUMERICAL ANALYSIS OF THE STEEP CIRCULAR
WAVEGUIDE TAPER

Figure E-1 shows a circular waveguide iris with steeply tapered sides. Each of these two sides can be thought of as a linear transition of length L. Experimental results for $L = 0$ can be found in Ragan's book (see the Reference list following the main text, Ref. 21, pp. 213–214). Figure E-2 shows these experimental results along with numerical results obtained using a nine-mode, mode-matching routine. The two abscissas in Figure E-2 represent the diameter of the waveguide aperture, and the two ordinates represent the reflection coefficient S_{11} magnitude and phase. It should be mentioned that Carin has previously investigated this device and has published results for the magnitude of S_{11} very similar to our own (Ref. 8), but no results for the phase of S_{11}. We have also generated results for $L = 001\lambda_o$ and $L = 10^{-9}\lambda_o$ where λ_o is the free-space wavelength at the operating frequency 9.375 GHz.

These data were generated taking into account nine modes and using two analytical techniques. First, boundary discretization and mode-matching were applied with 100 junctions between $z = 0$ and $z = L$. Second, the Galerkin's method version of the moment technique[4] was used with six cascaded sections and five triangle weighting functions per section. This procedure was executed at six iris diameters and, at each diameter, the results for S_{11} (mode-matching vs. method of moments, $L = 0,001\lambda_o$ vs. $L = 10^{-9}\lambda_o$) were indistinguishable; these data are shown in Figure E-3 along with the $L = 0$ mode-matching results. The nonzero L results converge to values close to the $L = 0$ results in magnitude and to values indistinguishable from the $L = 0$ results in phase.
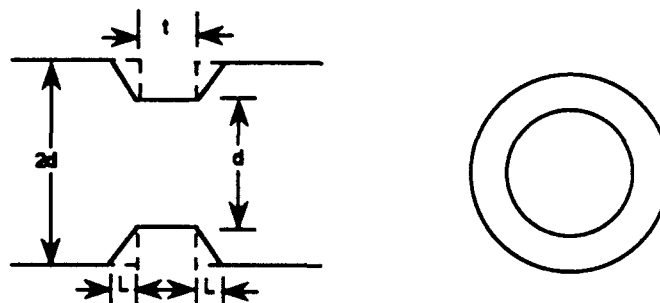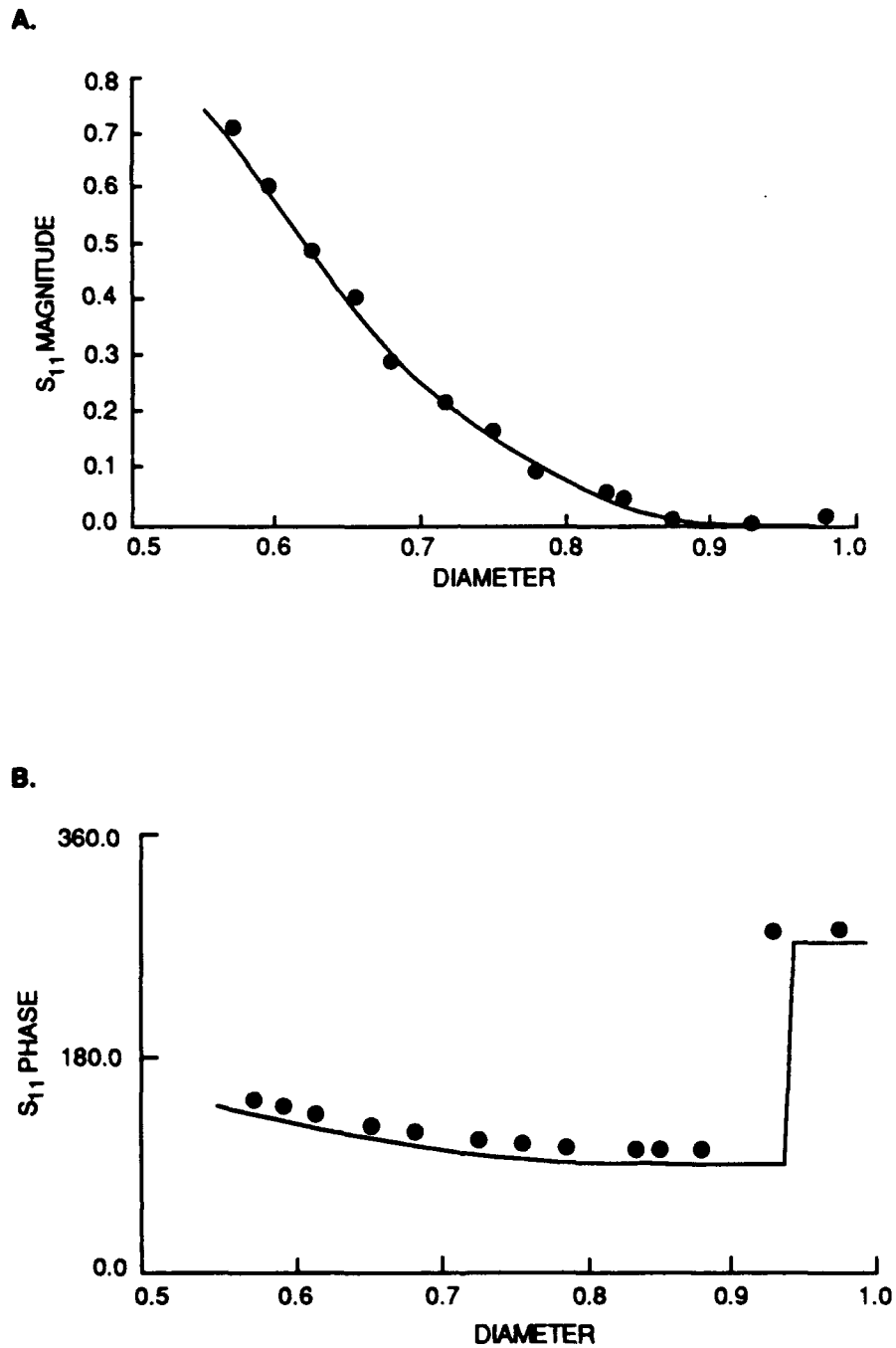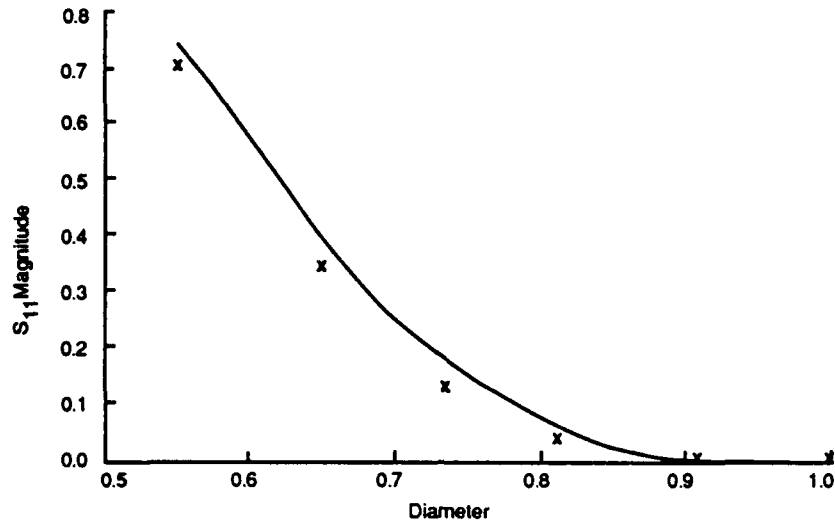

Figure E-1. Circular waveguide iris: 2d = 15/16 inch, t = 1/32 inch, frequency = 9.375 GHz.
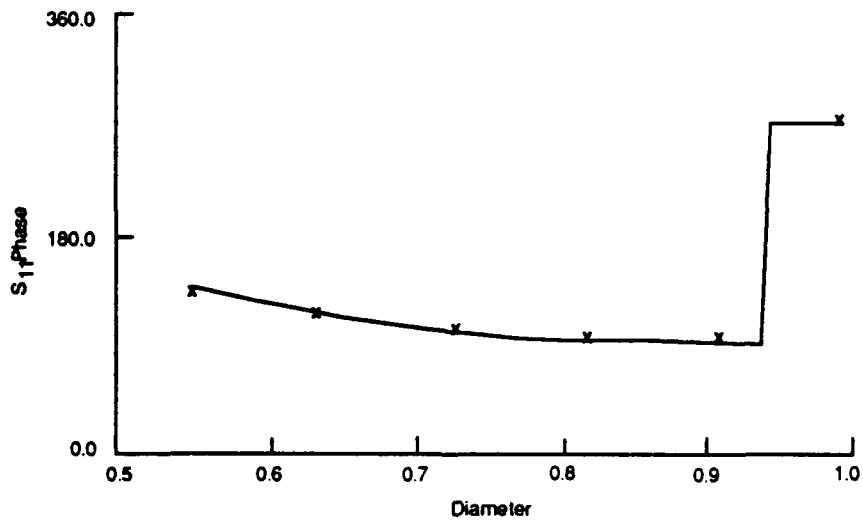
A.

B.

Figure E-2. Computed reflection coefficient for the circular iris of Fig. E-1 for the L = 0 case. The solid line was generated using mode-matching with nine modes. The dots were generated using experimental data from Reference 22. A. Magnitude, B. Phase.

A.

B.

Figure E-3. Computed reflection coefficient for the circular waveguide iris of Fig. E-1. The solid line was generated for the $L = 0$ case using mode-matching with nine modes. In addition, data were generated for $L = 0.001\lambda_0$ and $L = 10^{-9}\lambda_0$ using the moment method and the boundary discretization method. The same results (shown using crosses) were obtained for both lengths and both methods. A. Magnitude, B. Phase.

INITIAL DISTRIBUTION EXTERNAL TO THE APPLIED PHYSICS LABORATORY*

The work reported in TG 1379 was done under Navy Contract N00039-89-C-5301 and is related to Task BKHR9LXX F2B, supported by NAVSEA.

ORGANIZATION	LOCATION	ATTENTION	No. of Copies
DEPARTMENT OF DEFENSE			
Defense Technical Information Center	Alexandria, VA 23314	Accessions	12
DEPARTMENT OF THE NAVY			
Naval Air Systems Command	Washington, DC 22202	Library, Air 7226	2
Naval Sea Systems Command PMS 400B3	NC-2 Crystal City, VA	CAPT R. Cassidy	1
Naval Sea Systems Command	Washington, DC 22202	Library, Sea 9961	2
CONTRACTOR			
Antennas for Communications, Inc.	Ocala, FL	W. H. Riesz	1
UNIVERSITIES			
Polytechnic University	Farmingdale, NY	L. Carin	1
Purdue University	West Lafayette, IN	G. W. Slade	1
		K. J. Webb	2
NAVTECHREP	Laurel, MD 20723-6099		2
SPAWAR	Arlington, VA 20363-5100	Library	2

Requests for copies of this report from DoD activities and contractors should be directed to DTIC. Cameron Station, Alexandria, Virginia 22314 using DTIC Form 1 and, if necessary, DTIC Form 55.

*Initial distribution of this document within the Applied Physics Laboratory has been made in accordance with a list on file in the APL Technical Publications Group.